https://ntrs.nasa.gov/search.jsp?R=19830027618 2020-03-21T01:09:40+00:00Z

General Disclaimer

One or more of the Following Statements may affect this Document

- This document has been reproduced from the best copy furnished by the organizational source. It is being released in the interest of making available as much information as possible.

- This document may contain data, which exceeds the sheet parameters. It was furnished in this condition by the organizational source and is the best copy available.

- This document may contain tone-on-tone or color graphs, charts and/or pictures, which have been reproduced in black and white.

- This document is paginated as submitted by the original source.

- Portions of this document are not fully legible due to the historical nature of some of the material. However, it is the best reproduction available from the original submission.

Produced by the NASA Center for Aerospace Information (CASI)

JPL NO. 9950-867

Quarterly Report

DRL No. 162

DOE/JPL-956046-83/7
Distribution Category UC-63

TEM AND SEM (EBIC) INVESTIGATIONS OF SILICON BICRYSTALS

Quarterly Report

Period: April 1, 1983 to June 31, 1983

JPL Contract No. 956046, Report #7

Prepared by:

R.Gleichmann and D.G.Ast

Department of Materials Science and Engineering
Cornell University
Ithaca, NY 14853.

July 1983

The JPL Flat Plate Solar Array Project is sponsored by the U.S. Department of Energy and forms part of the Solar Photovoltaic Conversion Program to initiate a major effort towards the development of low-cost solar arrays. This work was performed for the Jet Propulsion Laboratory, California Institute of Technology by agreement between NASA and DOE.

(NASA-CR-173107) TEM AND SEM (EBIC) INVESTIGATIONS OF SILICON BICRYSTALS Quarterly Report, 1 Apr. - 31 Jun. 1983 (Cornell Univ.) 13 p HC A02/MF A01 CSCL 20B

N83-35889

Unclas
G3/76 36726

TEM AND SEM (EBIC) INVESTIGATIONS OF SILICON BICRYSTALS

Introduction

The production of low cost solar silicon involves a compromise between cell efficiency and crystalline perfection. An optimum trade-off between these two properties requires knowledge of the electrical effects of crystal defects, such as grain boundaries, in order to estimate their influence on cell efficiency. In most solar grade materials the dominant structural defects are dislocations and first order twins and the electrical properties of these defects have been studied previously. Due to the high growth speed, ribbon materials contain large residual stresses. The relaxation of these stresses can cause the generation of additional (sub) grain tilt boundaries and may even result in boundaries with large mis-orientation angles. Such boundaries usually are known to have a strong influence on the minority carrier lifetime due to their recombination activity. The aim of the present report was to study the electrical and structural properties of low and medium angle tilt grain boundaries in silicon bicrystals grown at JPL in order to obtain insight into the mechanisms determining the recomination activity. The electrical behavior of these grain boundaries was studied with the EBIC technique. Schottky barriers rather than p-n junctions were used to avoid annealing induced changes of the structure and impurity content of the as-grown crystals. The structure of the boundary was studied with transmission electron microscopy.

Experimental

Both bicrystal samples were grown at JPL and were oriented to obtain tilt boundaries with {100} median planes and <100> tilt axes. Tilt angles were about 20°, to study the effect of larger misorientations, and about 5° to study the

electrical properties of low angle tilt boundaries. The starting material was Czochralsky grown silicon (p-type, 4 Ω cm). The samples supplied by JPL were in the form of 1-1/2 inch diameter wafer of 1mm thickness. The wafers were mounted on glass plates and cut by a diamond saw into 8x12 mm stripes parallel to the boundaries. The stripes were mounted on a stainless steel polishing block with thermosetting wax and ground down with silicon carbide powder, starting with 600 grit and progressing to a 1200 grit, to a thickness of 100 um for TEM samples and 300 μm for EBIC samples. After a final polish with M305 powder, the TEM stripes were mounted on glass carriers and discs with 3mm diameter were cut by ultrasonic drilling. These discs were then thinned down by ion milling since the chemical etching preferential attacked the grain boundary plane. Stripes used for EBIC investigations were additionally polished on one side with syton. The stripes were cleaned using the RCA procedure and Schottky diodes were formed by evaporating 500 A of pure aluminum in a vacuum of better than 10^{-6} Torr. To limit the capacity of the Schottky diodes, 3x3 mm square dots were prepared by marking the samples with a metal grid carefully aligned parallel to the boundary. The TEM analysis was carried out with a JEM 200 CX operated at 160 keV and equipped with a side-entry double tilt stage for diffraction contrast experiments and tilt angle determinations. The EBIC investigations were carried out in a JEOL 733 SEM equipped with an additional low impedence amplifier (Keithley, model 427) and a special EBIC holder. To avoid image contributions from the depletion layer, i.e. to establish diffusion rather than drift field conditions, beam voltages above 20 kV were applied. The use of high beam voltages has the additional advantage that the onset of high injection conditions is shifted to higher beam currents. In solar material, high injection conditions can be reached relatively easily since the doping level is relatively low. The beam currents used in the present investigation were usually 0.1 nA. The EBIC image is formed by collecting the beam induced

minority charge carriers at the Schottky diode and using this current to modulate the intensity of a CRT display scanned synchronously with the specimen beam. Crystal defects reducing the lifetime of the material are characterized by an enhanced recombination activity and thus appear dark on the EBIC image.

Results and Discussion

TEM allows only the inspection of short pieces of the boundary which, at most, some ten micrometers in length. Within these limitations, the 20° boundary was found to be surprisingly straight, homogeneous and free of extrinsic dislocations. These features can be seen in the brightfield images of different parts of the boundary - Fig. 1. Since the density of the intrinsic dislocations is expected to be high with spacings in the order of 18 Å, it was not surprising that individual dislocations could not be resolved even in weak-beam micrographs.*

The relative orientation of the adjoining crystals was determined by diffraction analysis of adjacent parts of the bicrystal on either sides of the boundary and by selected area diffraction at the boundary itself. Weak convergent beam conditions were selected in order to enhance the visibility of the Kikuchi lines. One example of such pairs of diffraction pattern is given in Fig. 2. The upper crystal in the image was tilted close to a [001] orientation. The crystal orientation of the lower left part corresponding to this special orientation of the bicrystal was close to [0$\bar{1}$3]. The exact determination of the orientation relationship using Kikuchi lines gave the result that the tilt angle of the boundary was 17.2°±0.1°. The bicrystal contained no detectable

---

* The dislocations should lie paralell to the surface of the specimen. Unfortunately, α-fringes (having about the same orientation as the dislocation lines) cannot be avoided using diffraction contrast imaging. Some minor disturbances in the α-fringe appearance indicate some density variations in the dislocation array.

twist component. However, the selected area diffraction at the boundary plane (near edge on position) shows an additional tilt component about the [010] axis orthogonal to the wafer surface of 1.3°±0.2°. An analysis of the diffraction streak corresponding to the boundary plane indicated a boundary width in the order of 50 Å. This suggests that the boundary, whose orientation is half way between $\Sigma=25$ and Σ-37, may be facetted on a fine scale. It was difficult to orient the boundary precisely into an edge-on position. For this reason, the symmetric position of the boundary plane relative to the adjoining crystals was proved by exciting identical imaging conditions in both crystal parts (symmetric tilting out of the edge-on position) and measuring the image width at the same position of the boundary. Within the accuracy of the technique, about one degree, the boundary plane was identical to the median plane. The EBIC investigation showed that the boundary over a distance investigated, about one centimeter, was essentially straight (compare e.g. Fig. 3). Only minor variations in the order of few microns could be observed and the recombination efficiency along the boundary plane appeared to be homogeneous. The material adjacent to the boundary contained, however, a high density of extremely recombination active dislocations. The density of these dislocations was in the order of several $10^5 cm^{-2}$. The high dislocation density makes it difficult to obtain quantitative data on individual dislocations. However, strong recombination undoubtedly occurs at these dislocations. The strong recombination activity of the dislocations can be explained by their TEM appearance. All dislocations investigated were found to be heavily decorated with small precipitates and appear as "pearl chains". One brightfield and one darkfield image of the dislocations is given in Fig. 4. Fig. 4a shows in addition the presence of an isolated small precipitate. The weak-beam micrograph of Fig. 4b demonstrates that the decorating particles are composed

of a large number of smaller precipitates in the size range 20...100 Å decorating the dislocations asymmetrically. Unfortunately the amount of decoration is too small to obtain an X-ray signal of sufficient intensity to analyze their chemical composition, even when the STEM is highly focussed. However, the appearance of the precipitates resembles somewhat early precipitation of oxygen in silicon and may be a result of the low cooling rate during the growth of the bicrystal. Although no decorating precipitates could be observed at the boundary plane itself, it is likely that impurity segregated to the boundary and are present below the TEM detection limit.

The investigation of the second bicrystal which contained a low angle tilt boundary was carried out in an identical manner. The measured tilt angle was 5.5°±0.1°. Again, an additional tilt was observed around an axis orthogonal to the wafer surface ([010] orientation within the boundary plane) with a tilt angle of 2.1°±0.2°. Finally, a twist component of 0.7°±0.1° was also present in this boundary. The boundary appeared straight and homogeneous in the TEM and dislocations with varying spacings, from 100 to 1000 Å, could be observed (see Fig. 5). No evidence for impurity segregation could be found either at the boundary or at dislocations in adjacent crystal regions. The dislocation density in the bulk crystal was lower and about $1.10^{5}cm^{-3}$. This TEM result was verified by investigating larger areas with the EBIC technique. One example of a relative straight segment of the boundary is given in Fig. 6. The "sideways movements" or kinks of the boundary usually are below 10µm. The boundary seems to be instable, see Fig. 7, which shows a dissociation reaction of the boundary. The additionally introduced boundaries of dotted EBIC contrast correspond to the intersections of {111} planes with the surface and thus "intersections' appear to be first order twin boundaries. Dissociation of a low angle grain boundary containing twist and tilt components occur relatively frequently and similar reactions have been observed previously by Foell and Ast[1] and by Carter and

Foell[2]. First order coherent twins are known to have usually a very low recombination activity. Their main contrast arises from the presence of dislocations in the boundary plane[3] (Strunk and Ast). This interpretation is supported by the dotted appearance of the boundaries and the partly vanishing contrast, particularly at the start of the twin plane in the lower part. Though all the dislocations appeared to be clean within the resolution of the TEM, the high EBIC contrast of the dislocations indicates that in this sample, too, the dislocations are decorated. Decoration of the 5.5° boundary could account for the observed high recombination activity. The EBIC contrast depends on the imaging conditions but usually exceeds 50% as can be seen from the line scan across the boundary shown together with the zero current line, see Fig. 8. The line profile was taken at 30 keV (5.10^{-10} Å) to minimize the influence of the Schottky diode depletion region. The electrical asymmetry of the boundary is typical and could be observed at different positions and imaging conditions. Possible explanations are that the stress field of the boundary is asymmetric and/or that the impurity level in the adjoining crystals (at least in the neighborhood of the boundary) is different. As a general result of the investigation one can conclude that in these particular bicrystal samples the electrical effect of grain boundaries appears to be independent of the boundary misorientation. The dominant influence appears to be impurity segregation effects to the boundary. Cleaner bicrysals would be required to study intrinsic differences in the electrical activity of the two boundaries.

REFERENCES

1. H. Foll and D.G. Ast, Phil. Mag. A 40 (1979) 589.
2. C.B. Carter and H. Foll "Dislocation Modelling in Physical Systems" Eds. M.F. Ashby, R. Bullough, C.S. Hartley and J.P. Hirth, 1980 (Pergamon, Oxford).
3. H. Strunk and D.G. Ast, 38 Proc. Electron Microscopy Soc. Amer. Eds. B.W. Bailey, 1980, p. 332.

FIGURE CAPTIONS

Fig. 1. Brightfield TEM micrographs of the 17.2° tilt boundary, taken from several TEM specimen prepared from the bicrystal (tilt axis [100]).

Fig. 2. Determination of the orientation relationship of the 17.2° boundary by convergent beam diffraction.

Fig. 3. EBIC micrograph of the 17.2° tilt boundary at 20 keV.

Fig. 4. Brightfield (a) and darkfield weak-beam image of the dislocations in the bulk section of the 17.2° bicrystal.

Fig. 5. Darkfield weak-beam image of the 5.5° tilt boundary with the common (100) reflections excited.

Fig. 6. Straight segment of the 5.5° tilt boundary imaged with EBIC, beam energy is 20 keV.

Fig. 7. Dissociation reaction of the 5.5° boundary (EBIC, 30 keV).

Fig. 8. Line scan across the 5.5° tilt boundary with corresponding zero line (area corresponding to Fig. 6) taken at 30 keV.

ORIGINAL PAGE IS
OF POOR QUALITY

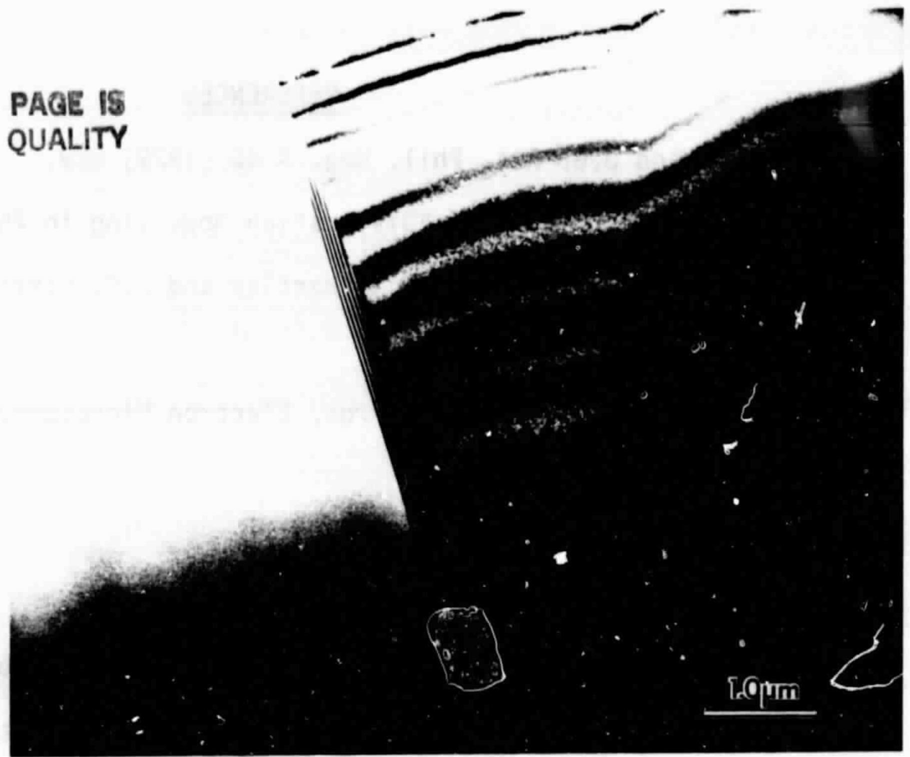

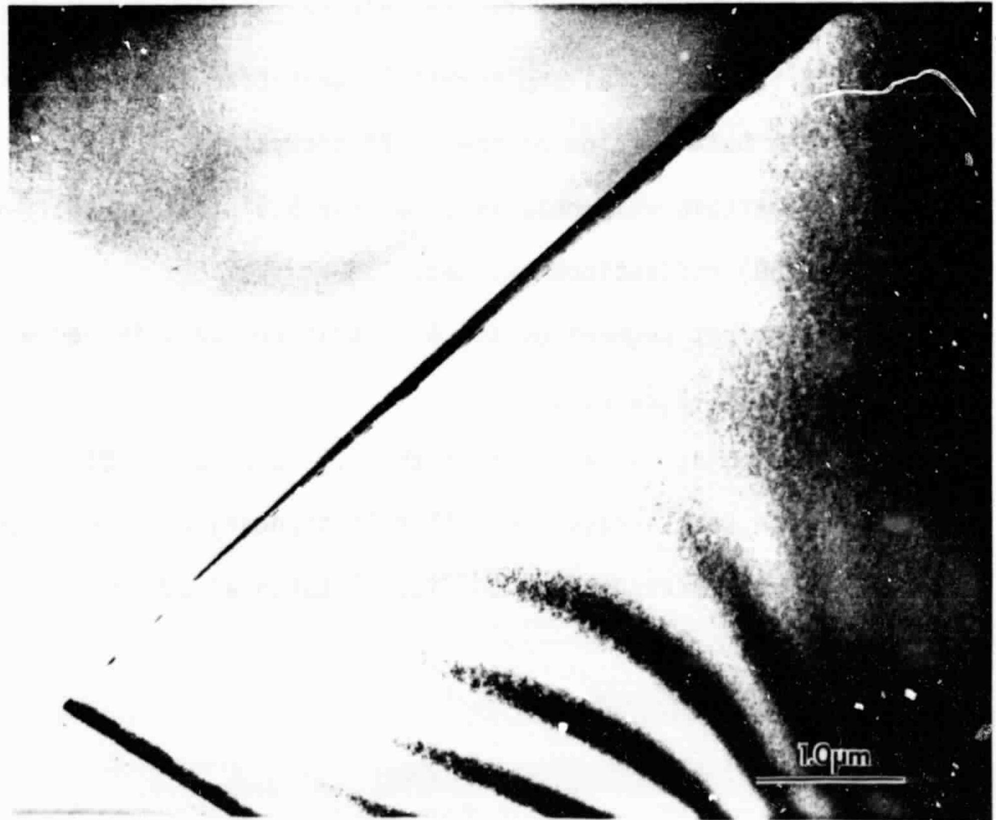

1

ORIGINAL PAGE IS
OF POOR QUALITY

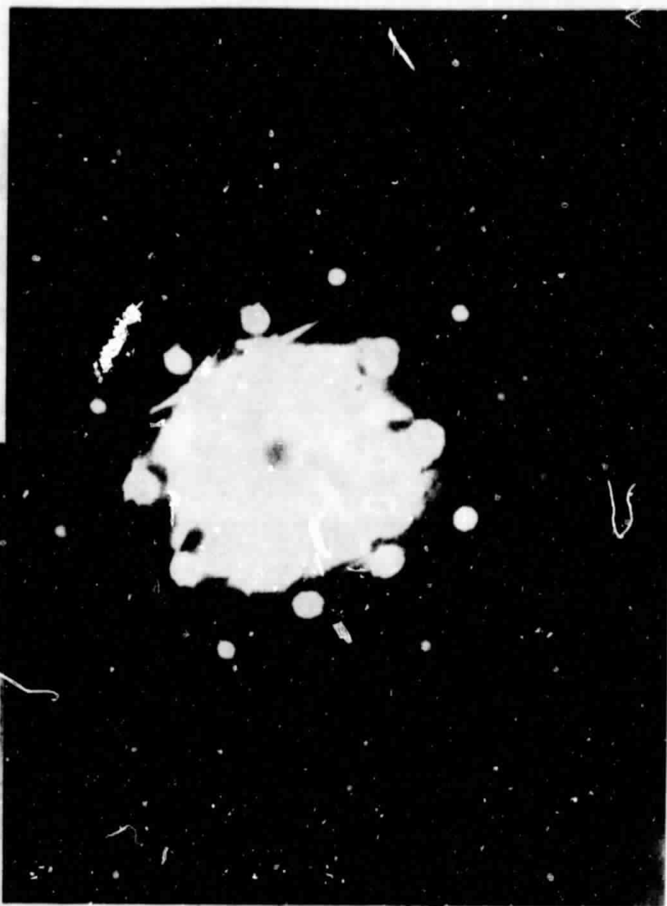

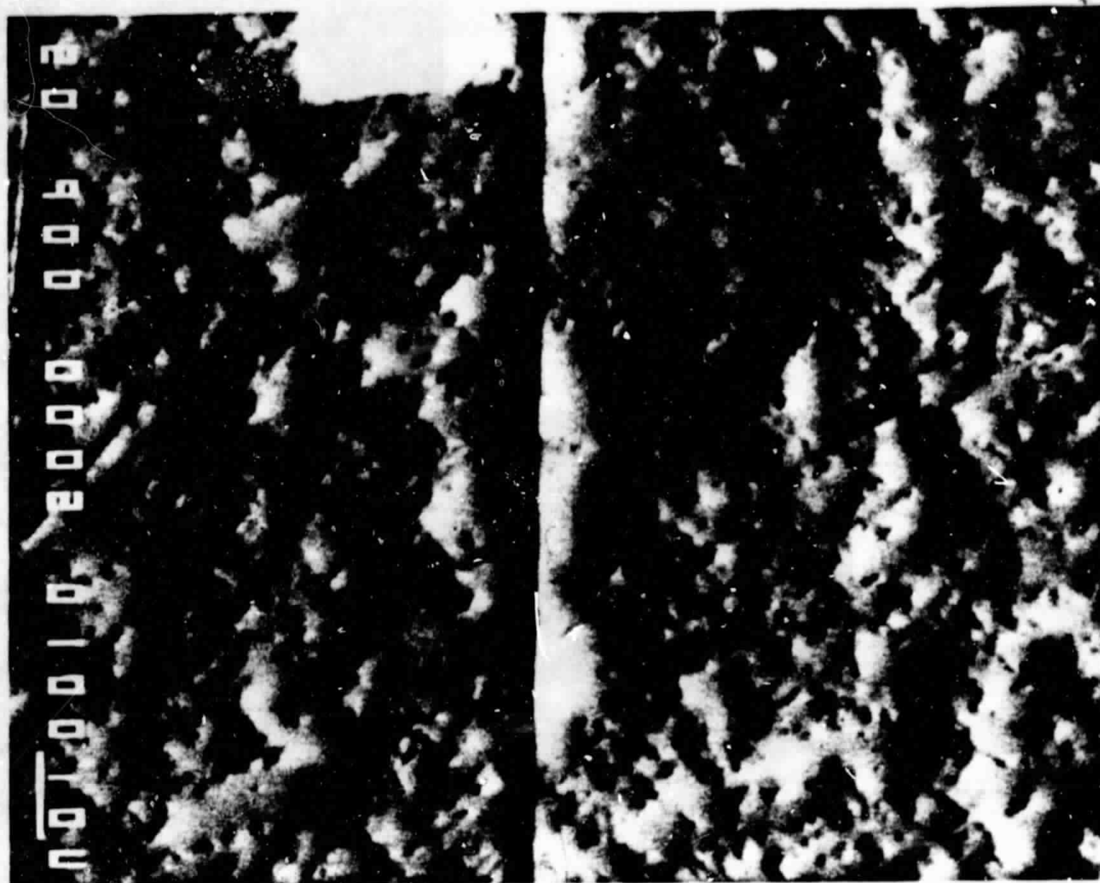

3

ORIGINAL PAGE IS
OF POOR QUALITY

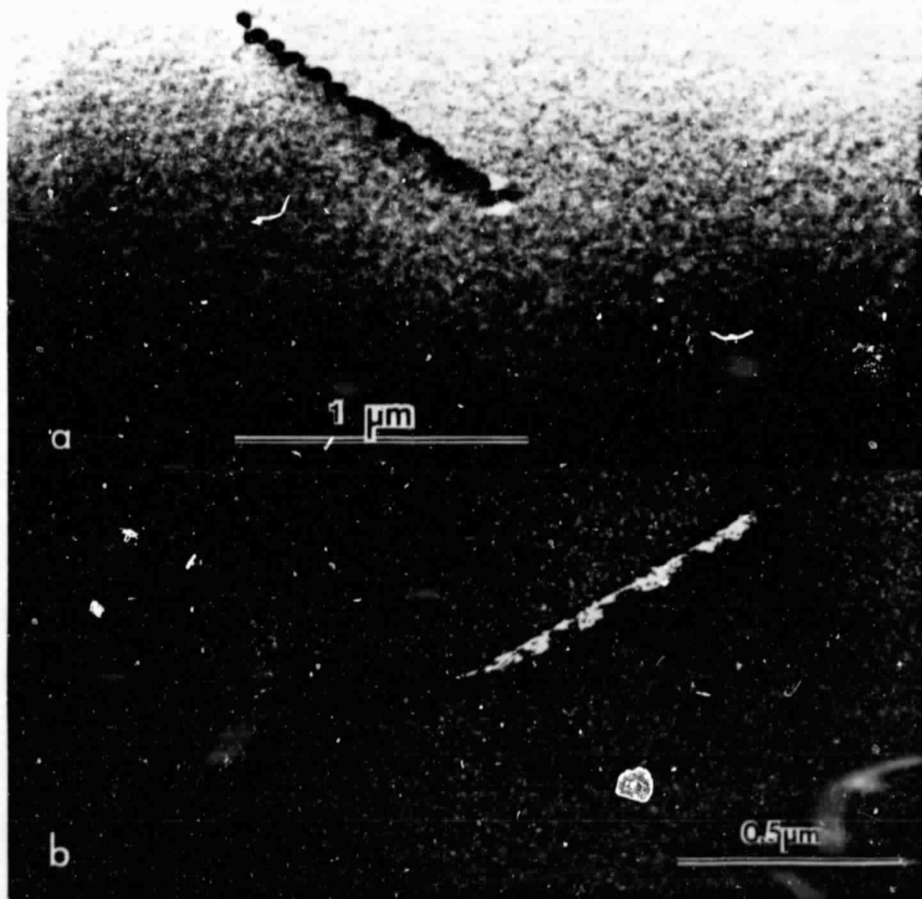

4

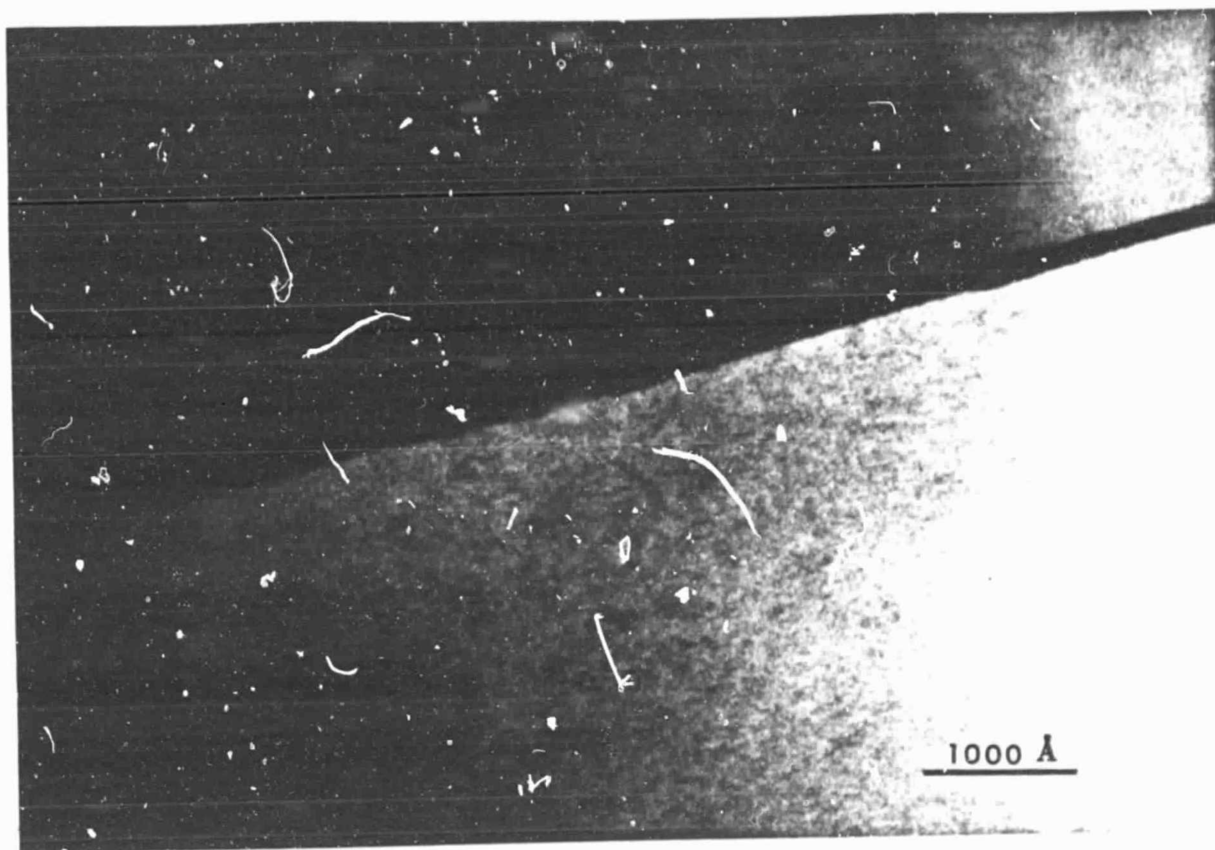

5

ORIGINAL PAGE IS
OF POOR QUALITY

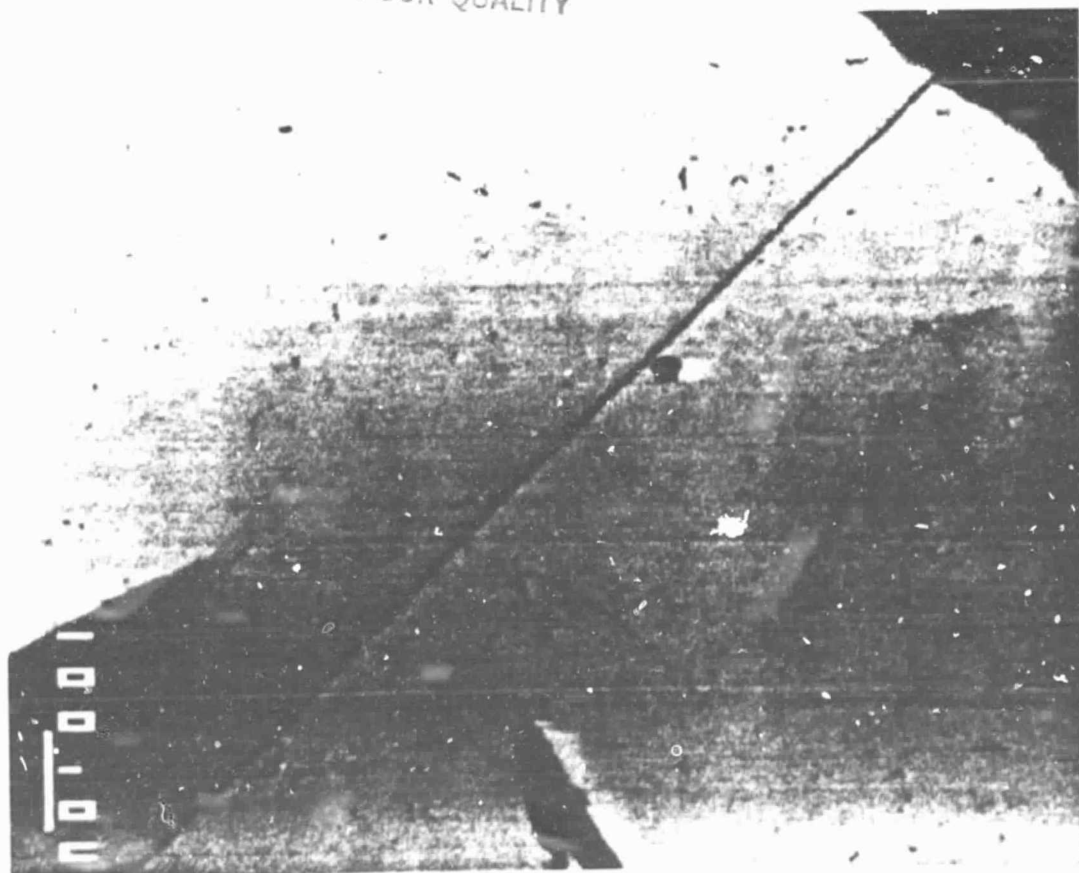

6

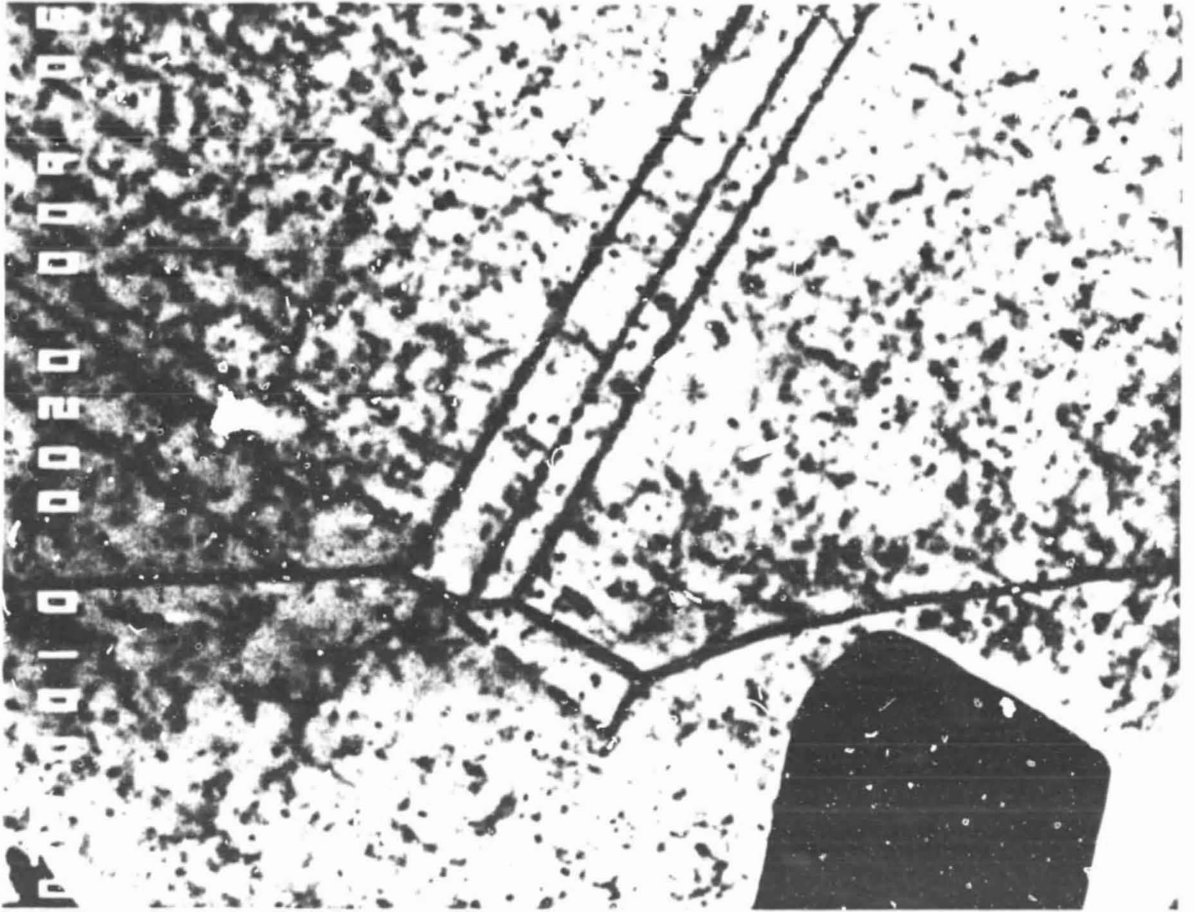

7

ORIGINAL PAGE IS
OF POOR QUALITY

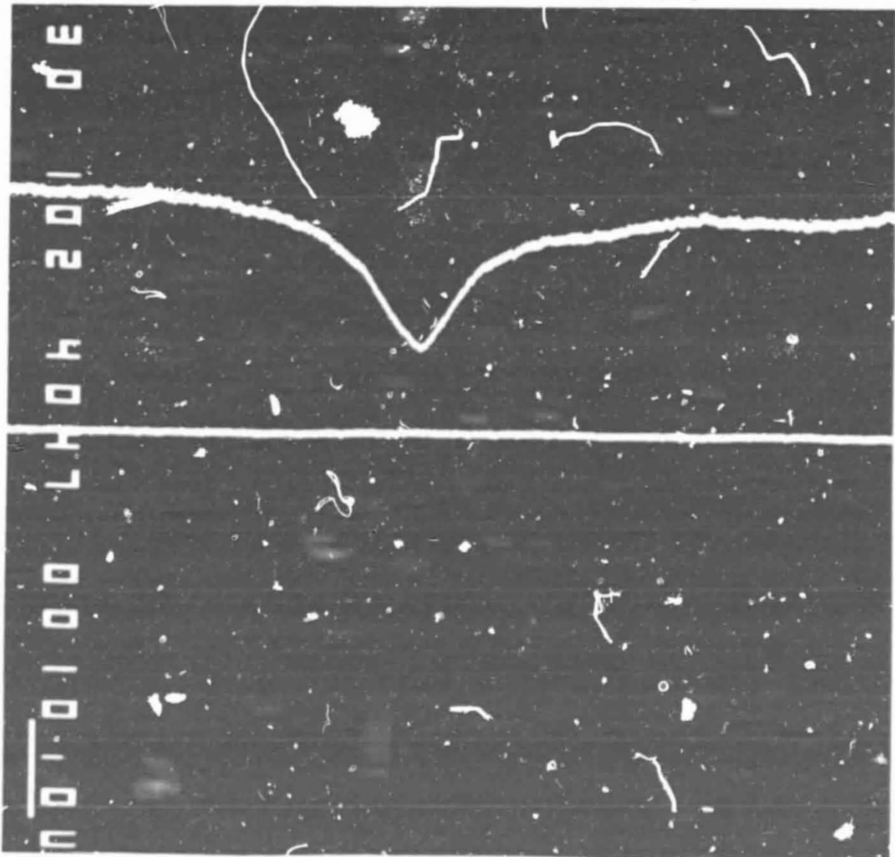

8